Cell Chemical Biology

SynPull: An advanced method for studying neurodegeneration-related aggregates in synaptosomes using super-resolution microscopy

Graphical abstract

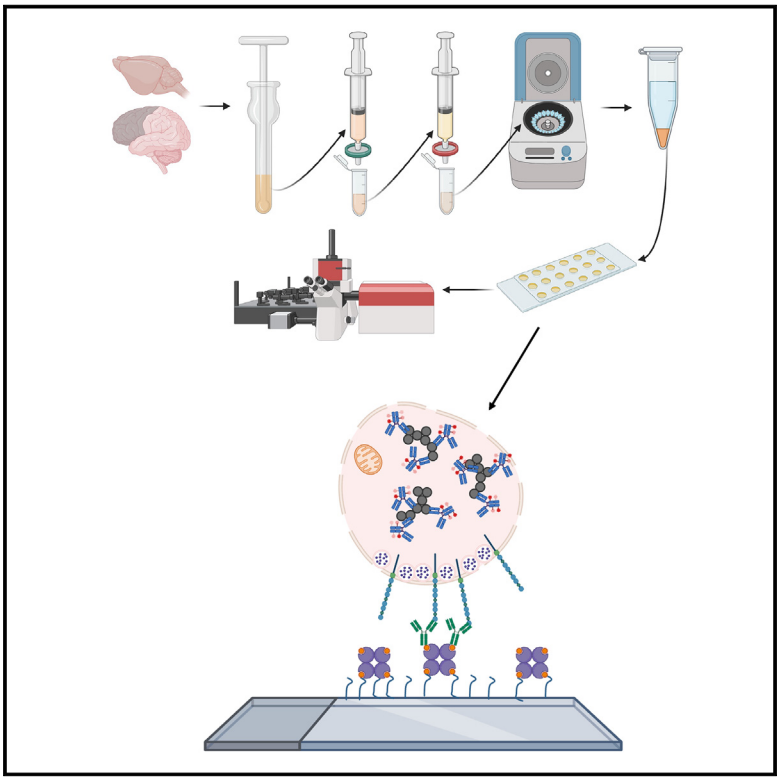

Authors

Shekhar Kedia, Emre Fertan, Yunzhao Wu, ..., Maria Grazia Spillantini, John S.H. Danial, David Klenerman

Correspondence

jshd1@st-andrews.ac.uk (J.S.H.D.), dk10012@cam.ac.uk (D.K.)

In brief

Connections between nerve cells are highly damaged in Alzheimer's and Parkinson's disease. This is believed to be linked to the formation of small-soluble aggregates of disease-related proteins. Here, Kedia et al. develop a method to study these aggregates using a combination of advanced surface-chemistry, microscopy, and computational analysis techniques.

Highlights

- A method is developed and validated for studying protein aggregates in synaptosomes
- Aβ, tau, and αSyn aggregates are characterized in AD and PD synapses
- AT8-positive tau is the predominant aggregate in Alzheimer's disease synaptosomes
- Aβ and αSyn aggregates inside the synaptosomes are bigger than the ones outside

Kedia et al., 2025, Cell Chemical Biology *32*, 338–351
February 20, 2025
https://doi.org/10.1016/j.chembiol.2025.01.001

CellPress

CellPress
OPEN ACCESS

Cell Chemical Biology

Technology

SynPull: An advanced method for studying neurodegeneration-related aggregates in synaptosomes using super-resolution microscopy

Shekhar Kedia,[1,2,7] Emre Fertan,[1,2,3,7] Yunzhao Wu,[1,2] Yu P. Zhang,[1,2] Georg Meisl,[1,2] Jeff Y.L. Lam,[1,2] Frances K. Wiseman,[4,5] William A. McEwan,[2,3] Annelies Quaegebeur,[3] Maria Grazia Spillantini,[3] John S.H. Danial,[1,2,6,*] and David Klenerman[1,2,8,*]

[1]Yusuf Hamied Department of Chemistry, University of Cambridge Cambridge CB2 1EW, UK
[2]UK Dementia Research Institute at University of Cambridge Cambridge CB2 0XY, UK
[3]Department of Clinical Neurosciences, University of Cambridge Cambridge, UK
[4]UK Dementia Research Institute at University College London London NW1 3BT, UK
[5]Queen Square Institute of Neurology, University College London London WC1N 3BG, UK
[6]School of Physics and Astronomy, University of St Andrews St Andrews KY16 9SS, UK
[7]These authors contributed equally
[8]Lead contact
*Correspondence: jshd1@st-andrews.ac.uk (J.S.H.D.), dk10012@cam.ac.uk (D.K.)
https://doi.org/10.1016/j.chembiol.2025.01.001

SIGNIFICANCE Synaptic dysfunction and loss are key pathologies in neurodegenerative disorders such as Alzheimer's disease and Parkinson's disease. The rate of synaptic decline correlates strongly with other changes such as cognitive loss and behavioral abnormalities. The protein aggregation associated with these diseases causes synaptic pathology. However, the current methodologies to study these proteins in the synapse are limited. We have developed and validated SynPull as a method to characterize the protein aggregates inside the synapse at great resolution and detail. By using specific targets to capture the synaptosomes, we have improved the specificity of the method. This will enable the study of sub-populations of synapses selectively affected in various diseases. SynPull is therefore a useful method for researchers studying synaptic proteins in health and disease.

SUMMARY

Synaptic dysfunction is a primary hallmark of both Alzheimer's and Parkinson's disease, leading to cognitive and behavioral decline. While alpha-synuclein, beta-amyloid, and tau are involved in the physiological functioning of synapses, their pathological aggregation has been linked to synaptopathology. The methodology for studying the small-soluble protein aggregates formed by these proteins is limited. Here we describe SynPull, a method combining single-molecule pull-down, super-resolution microscopy, and advanced computational analyses to characterize the protein aggregates in human and mouse synaptosomes. We show that AT8-positive tau aggregates are the predominant aggregate type in synaptosomes from postmortem Alzheimer's disease brain, although the aggregate size does not change in disease. Meanwhile, the relatively smaller amount of alpha-synuclein and beta-amyloid aggregates found in the synapses are larger than the extra-synaptic ones. Collectively, these results show the utility of SynPull to study pathological aggregates in neurodegeneration, elucidating the disease mechanisms causing synaptic dysfunction.

INTRODUCTION

Alzheimer's and Parkinson's disease (AD and PD) collectively make-up more than half of all neurodegenerative disorder cases. Both are neuropathologically characterized by increased inflammation, oxidative stress, and the abnormal accumulation and aggregation of beta-amyloid (Aβ) and hyperphosphorylated (p)tau[1,2] in AD, and alpha-synuclein (αSyn)[3,4] in PD. Another common pathology seen in both diseases is progressive synaptic dysfunction, leading to cognitive and behavioral deficits. In both diseases pathological aggregates of the proteins mentioned previously have been linked to synaptic dysfunction.[5–7]

The presence and role of Aβ in the synapse is an area of active research, with some evidence suggesting a role in neuronal function, especially in times of increased synaptic activity, during which Aβ production is increased.[8] When neurons were treated with β- and γ-secretase inhibitors, increased neuronal loss was observed, which could be ameliorated by Aβ40 treatment.[9] Soluble N-ethylmaleimide sensitive factor attachment receptors (SNARE) complexes are reduced in postmortem AD brains[10] as well as mouse models,[11] indicating synaptic dysfunction in AD. Interestingly, the total amount of synaptobrevin, syntaxin-1, or SNAP-25, which are components of the SNARE complex, are not altered, suggesting that Aβ inhibits the formation of the SNARE complex. Indeed, Yang et al.[11] showed direct binding of oligomeric Aβ to syntaxin-1, altering SNARE complex formation. The presence of Aβ is not only limited to the pre-synapse, as it has been shown that Aβ can interact with post-synaptic neuroligin (NLGN)1, leading to Aβ oligomer formation.[12] Thus, while Aβ may be a physiological component of all synapses, formation of pathological Aβ aggregates with different sizes and structures may shift its role from physiological to pathological and promote synaptic loss. Therefore, quantifying and characterizing Aβ aggregates in the synapses will be a valuable method for identifying novel pathological AD-related mechanisms.

Similarly, the presence of pTau in the synapse has also been studied. Frandemiche et al.[13] showed tau is localized in the axonal shafts in healthy neurons during resting conditions and synaptic activity relocated tau to the synaptic terminals, interacting with actin. However, in the presence of oligomeric Aβ, tau was translocated to the synapse in the resting state and both tau and actin levels were decreased after synaptic activity, suggesting an Aβ-dependent synaptic dysfunction caused by tau. Moreover, it has also been suggested that tau can interfere with synaptic vesicles. AT8-positive tau can bind to synaptic vesicles through its N-terminal domain and hinder presynaptic function, including synaptic vesicle mobility and release.[14] Moreover, tau can spread between neurons via synaptic transmission[15] and synaptic accumulation of oligomeric tau, in the absence of fibrillar species, has been reported in early AD, suggesting the involvement of these small-soluble aggregates in synaptotoxic processes.[16]

Lastly, αSyn is a synaptic protein required for synaptic function and neurotransmitter release, through its involvement in the SNARE complex formation by interacting with synaptobrevin.[17] However, when αSyn starts to aggregate, the formed oligomers recruit the synaptic complex proteins[18] and inhibit neurotransmitter vesicle docking and release.[19,20] While the Lewy bodies are the most recognized form of αSyn accumulation in PD and other synucleinopathies, recent studies have shown that the earlier forms of soluble αSyn aggregates may be more toxic than the Lewy bodies.[21] Our group has recently shown that the size and shape of the αSyn aggregates, most of which are below the diffraction-limit of light, differs as the disease progresses and influences their toxic properties[22] making it essential to study αSyn aggregates in the synapse.

As explained above, pathologically aggregated Aβ, pTau, and αSyn are all associated with synaptic dysfunction. The smaller, oligomeric aggregates formed by these proteins, rather than the larger and insoluble plaques, tangles, and Lewy bodies may be the highly toxic forms, promoting synaptic loss. The sub-diffraction limit size, low abundance in the synapse, and high heterogeneity of these aggregates makes it difficult to study and characterize them[23] using traditional methods such as immunohistochemistry. Along with electrophysiology, one of the most valuable tools for studying synaptic pathology is synapto(neuro)somes.[24] First used by Catherine Hebb and Victor Whittaker,[25] synaptosomes are spherical membrane bound structures with a diameter ranging from 0.6 to 2 μm, made of nerve endings torn from the axon containing the synaptic boutons with neurotransmitter vesicles, synaptic proteins, mitochondria, and fragments of post-synaptic density. While synaptosome preparations has been successfully used to study synaptic pathology in neurodegenerative diseases,[26–30] to date, highly reproducible methods of reliably capturing synaptosomes and studying the sub-diffraction limit soluble toxic aggregates inside them has been limited.[16,31] Here, we developed and validated SynPull, as a method of studying synaptosomes with single-molecule pull-down (SiMPull), by selectively anchoring them to the surface using specific proteins of interest, and super-resolution microscopy, enabling the specific characterization of Aβ, tau, and αSyn aggregates in terms of number, size, and shape from postmortem human brain samples as well as mouse models of AD, tauopathy, and PD (Graphical abstract). By targeting specific synaptic proteins to immobilize synaptosomes on the surface and applying single-molecule detection techniques to aggregates located inside synaptosomes, SynPull opens up research avenues to study the role of pathological aggregates in synaptic dysfunction.

DESIGN

Our primary aim in developing SynPull was to isolate synaptosomes from postmortem human brains with AD and PD pathology, as well as mouse models of these neurodegenerative conditions, selectivity anchor them to an imaging surface, and to characterize the small-soluble αSyn, Aβ, and AT8-positive tau aggregates within these synaptosomes. Since these aggregates are below the diffraction-limit of light, low in abundance, and highly heterogeneous in terms of their morphology and presence in the synaptosomes, special single-molecule detection methods were used in combination with computational tools, to reliably characterize these pathological aggregates. We utilized the SiMPull methodology to specifically capture synaptosomes containing synaptic material, rather than liposomes formed by the re-fusion of lipid bilayer structures after the tissue homogenization steps. Since the density of these two products of tissue homogenization may be similar, we have utilized synapse-specific proteins (in this case Neurexin 1) to selectively localize the synaptosomes on the surface, instead of density gradient centrifugation-based methods to enrich for synaptosomes. One advantage of this approach is the possibility of changing the protein of interest to target for capture, in order to enrich for specific synaptosome sub-populations. For example, in conditions such as autism spectrum disorder, the composition of the synaptic proteins is altered, leading to pathological outcomes.[32] SynPull can be used to target the altered synapses specifically to further study the proteins inside them. We combined this approach with direct-stochastic optical

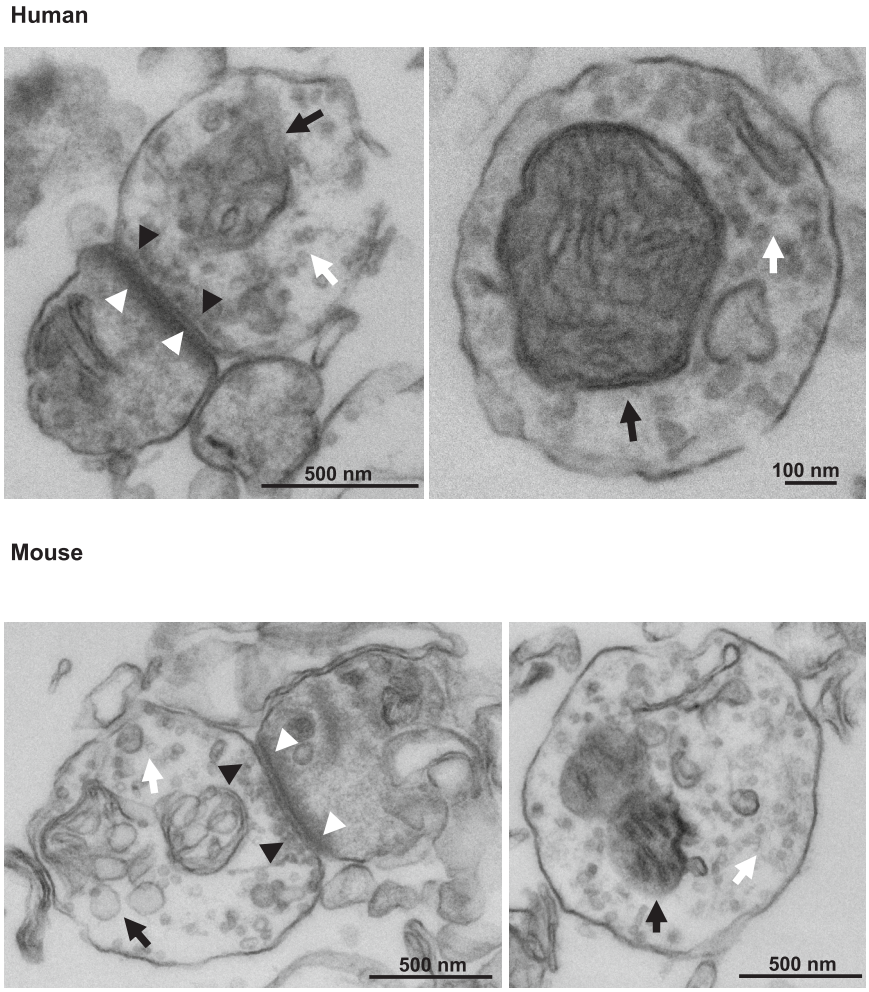

Figure 1. Transmission electron micrographs of synaptoneurosome (left) and synaptosome (right) preparations

The top panel shows micrographs from human control (no disease) samples, while the bottom panel presents micrographs from mouse (C57Bl/6J) synaptoneurosomes. Intact synaptoneurosomes are observed showing key morphological features including synaptic vesicles and mitochondria containing sealed presynaptic terminals and postsynaptic zone characterized by a synaptic junction with a postsynaptic density. The black arrowheads point at the presynaptic active zone while white arrowheads at the post synaptic density. The black arrows show mitochondria while the white arrows indicate numerous synaptic vesicles.

reconstruction microscopy (*d*STORM), which has previously been used to study tau aggregates inside the synaptosomes.

RESULTS

Electron microscopy studies

To confirm the integrity of isolated synapto(neuro)somes, electron microscopy (EM) was performed on synaptosome preparations from mouse and human brains. As shown in Figure 1, synaptoneurosomes containing post-synaptic compartments and synaptosomes with pre-synaptic boutons were successfully prepared from the human cortex (Figure 1A) and C57Bl/6J mouse cerebrum (Figure 1B). Morphological features, such as synaptic vesicles, synaptic membranes, and mitochondria observed in these micrographs validate the integrity of the isolated synapto(neuro)somes.

Control studies

In order to validate SynPull and test the suitability of the SiMPull surface for our experiments, we performed a number of control experiments (Figures 2A and S1). The results of these experiments and the ones we performed to characterize the synaptosomes from human and mouse brains are analyzed and presented using 95% confidence intervals (CI_{95}). This value, calculated using the difference between the group means represents the magnitude of difference between groups; while the inclusion of zero within the CI_{95} indicates no significant difference between the groups, CI_{95} values without zero indicate a statistically meaningful difference.[33]

Throughout our experiments, synaptosomes within the field of view were identified by the CellMask signal (diameter between 0.7 and 2.2 μm). Since the 561 nm (green) laser is used to excite the CellMask, it was crucial that the surface is not auto-fluorescent under illumination at this wavelength. When the surface was treated with all the steps required for the experiment, including neutravidin, polymer, neurexin (NRXN)1 capture antibody, fixing, and permeabilising, but no sample and CellMask added, no signal was detected under illumination with the 561 nm laser (CI_{95} = 21.14, 30.81), confirming the suitability of the SiMPull surface for studying synaptosomes, without significant background (noise) signal (Figures 2A and S1A). The next question concerned the fluorescence properties of the synaptosomes. Since most brain tissue samples are auto-fluorescent,[34] which may confound the signal acquired from immunolabeling, we aimed to test if the synaptosomes also fluoresce under light excitation, without any fluorophore labeling. No significant signal was detected from the mouse (CI_{95} = 21.14, 30.81) or human (CI_{95} = 2.83, 9.18) synaptosomes in the absence of CellMask (Figures 2A and S1B). Binding properties of CellMask to the SiMPull surface was also a concern, since unspecific binding could confound the signal. To test this, we compared the signal acquired with or without synaptosomes, in the presence of CellMask and observed significantly less signal from CellMask in the absence of synaptosomes (CI_{95} = 25.64, 36.95; Figures 2A, S1C, and S1D). Collectively, these results showed that neither the SiMPull surface, nor the synaptosomes emit any signal on their own and a label (CellMask) is necessary to identify the synaptosomes. Moreover, CellMask does not show unspecific binding to the SiMPull

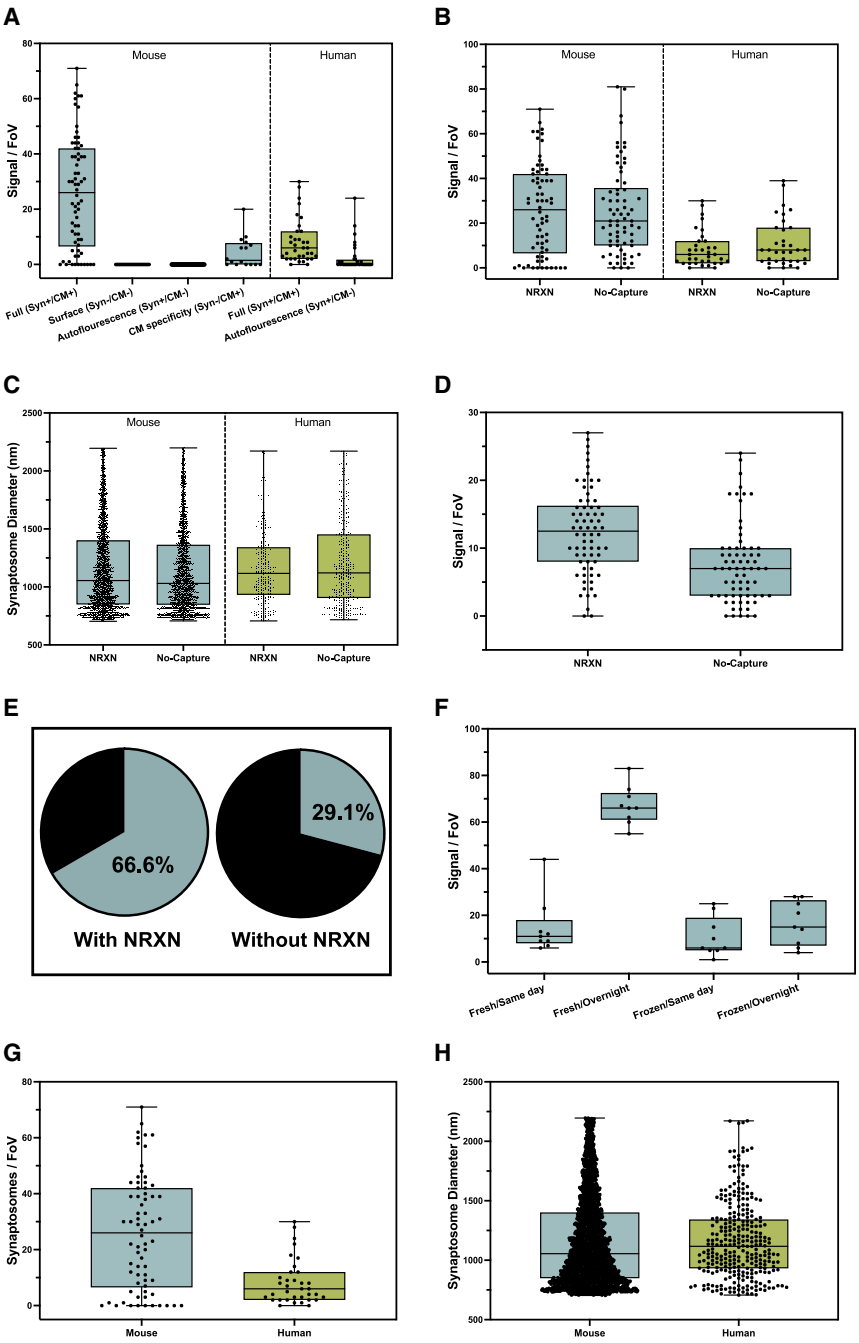

Figure 2. Control studies

(A) Neither the SiMPull surface nor the synaptosomes are auto-fluorescent, and CellMask does not non-specifically bind to the surface.

(B–E) (B) The number and (C) diameter of the CellMask-positive signal does not differ between the anti-neurexin captured and un-captured samples, however (D) Bassoon signal is higher in the anti-neurexin captured samples and (E) a higher percentage of the synaptosomes were bassoon positive, indicating higher synaptosome localisation on the SiMPull surface when the anti-neurexin capture is used.

(F) Freezing the synaptosomes decreases the signal, while overnight incubation on the SiMPull surface at 4°C increases the signal.

(G and H) (G) While the same mass of mouse brain tissue yield a higher number of synaptosomes, (H) the diameter of the synaptosomes does not differ between human and mouse brain tissue. Three independent experiments using different brain samples and SiMPull coverslips were performed, and the data were collected for a total of 70 fields of views.

surface. As such, the SynPull methodology with CellMask is well suited to study synaptic fragments.

To study the efficiency of capturing the synaptic fragments with an anti-NRXN1 antibody, we quantified the CellMask signal and measured synaptosome size, as well as the bassoon signal, with and without capture antibody. There was no significant difference between CellMask signal for mouse (CI_{95} = −6.32, 7.06) or human (CI_{95} = −7.06, 1.86) samples (Figure 2B), and the average synaptosome diameter did not differ considerably for mice (CI_{95} = 0.06, 45.33) or humans (CI_{95} = −96.94, 8.32; Figure 2C). However, the bassoon signal with anti-NRXN antibody was significantly higher (CI_{95} = 2.90, 6.98; Figures 2D and S1E) and a significantly higher percentage of synaptosomes in each field of view was bassoon positive (CI_{95} = 30.16, 44.85; Figure 2E) in the samples captured with the anti-NRXN antibody, suggesting the specific capturing of synapses and not liposomes when a capture antibody is used.

We concluded the control experiments by determining the effects of varying incubation and storage conditions on the synaptosomes and comparing the tissue samples from mouse models of neurodegeneration and human postmortem pre-frontal cortex tissue samples. While freezing the sample after preparing the synaptosomes decreased the yield significantly (CI_{95} = 41.74, 59.37), incubating the sample on the surface overnight at 4°C increased the signal (CI_{95} = 41.95, 62.50), suggesting that the optimal condition for capturing and imaging synaptosomes is to use them fresh with an overnight incubation (Figure 2F). Even though mouse and human synaptosome samples were prepared from a similar amount of tissue (~300 mg), a significantly higher number of synaptosomes were obtained from the mice (CI_{95} = 12.21, 23.22; Figure 2G), but synaptosome size did not differ between the species (CI_{95} = −39.96, 39.75; Figure 2H).

Aggregates in human brain samples

After establishing the optimal SynPull assay conditions, we compared the length, area, and eccentricity of the αSyn, Aβ,

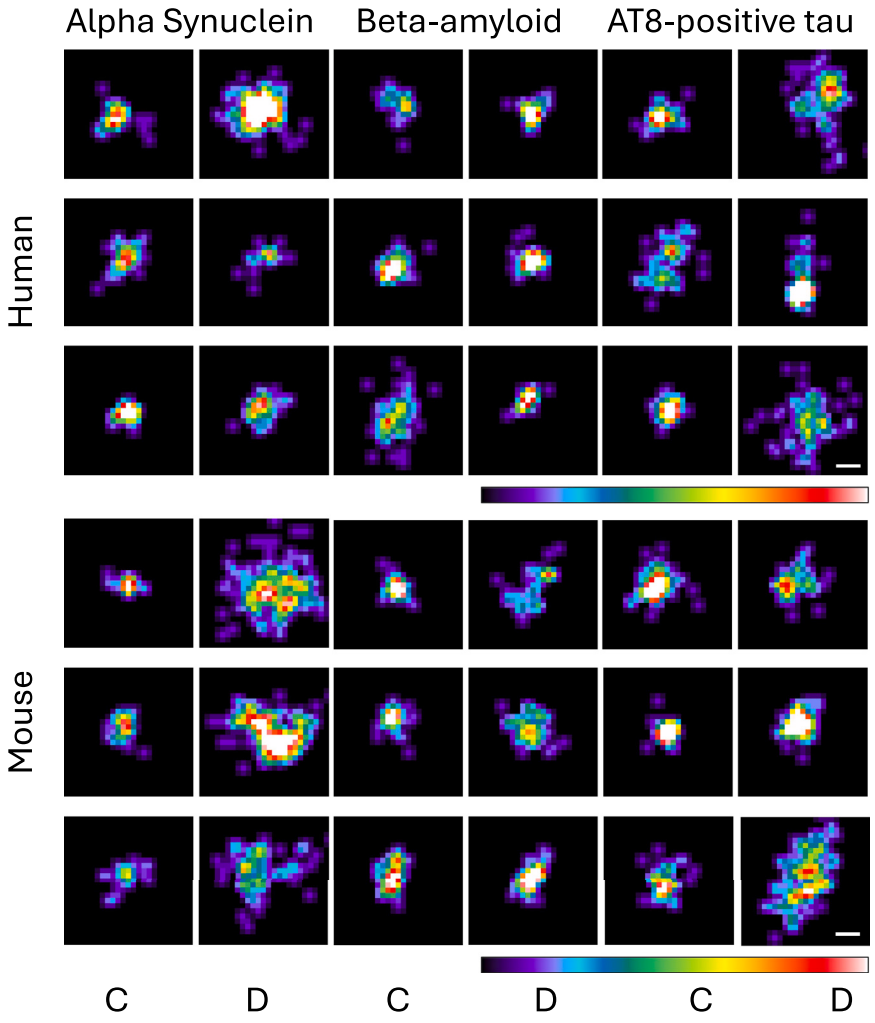

Figure 3. Representative pseudo-color images of alpha-synuclein, beta-amyloid, and AT8-positive tau aggregates from human and mouse brain samples acquired by *d*STORM and reconstructed by ACT software

The intensity is pseudo-color coded from black (minimum) to white (maximum). Columns labeled C contain images from control samples and the columns labeled D contain images from disease samples. Scale bars are 50 nm.

and AT8-positive tau aggregates from postmortem PD, AD, and control orbitofrontal cortex samples using *d*STORM (see Table S1 for statistical tests). Clusters with centroids within the synaptosomes were tagged as synaptic aggregates, meanwhile the ones still captured on the SiMPull surface yet located outside a synaptosome were defined as extra-synaptic aggregates. Overall, AT8-positive tau formed the longest aggregates, with an average length close to 150 nm, which were ~50 nm longer than the aggregates formed by αSyn and Aβ (see Figure 3 for representative images). Notably, the Aβ and tau aggregates were always characterized in the synaptosomes harvested from the same human brain samples.

The majority of the αSyn, Aβ, and AT8-positive tau aggregates were extra-synaptic, with relatively less number of aggregates inside the synaptosomes. While 3.7% of the synaptosomes from the control brains contained at least one αSyn aggregate, 16.5% of the synaptosomes from the PD brains contained one or more aggregates (CI_{95} = −39.50, 13.97). Meanwhile, 3.8% of the synaptosomes from the control brains contained at least one Aβ aggregate and this value was 3.1% for the synaptosomes from AD brains (CI_{95} = −8.68, 7.38). On the other hand, a significantly higher portion of synaptosomes from the AD brains contained one or more AT8-positive tau aggregates (87.5%), compared to the ones from the control brains (10.4%; CI_{95} = 67.57, 86.52).

For αSyn and Aβ, the number of aggregates inside or outside the synaptosomes did not differ between the PD/AD and control brains (Figures 4A and 4F), however the AD brain contained significantly more AT8-positive tau aggregates, both inside (factor of ~4.5) and outside the synaptosomes (factor of ~3,000; Figure 4K). Meanwhile, the length (160 nm vs. 80 nm; Figure 4B) and area (2640 nm^2 vs. 738 nm^2; Figure 4C) of the synaptic αSyn aggregates from the PD brain were bigger than the extra-synaptic aggregates from the PD and control brain. For Aβ, once again the synaptic aggregates were longer than the extra-synaptic ones (141 nm vs. 83 nm). However, the aggregates from the control brain had a size distribution with a longer mean (Figure 4G), although there were very few synaptic aggregates in the control brain, they were the longest and largest of the four conditions with an average length of 295 nm and average area of 7600 nm^2 (Figure 4H). On the other hand, the AT8-positive tau aggregates from the same samples did not show a length difference based on AD status inside the synapse, but the extra-synaptic aggregates were longer in the AD brain, compared to the controls (150 nm vs. 100 nm; Figure 4L), yet the area of the AT8-positive tau aggregates did not differ between the AD and control samples (Figure 4M).

The shape of the aggregates (circular or elongated) also differed between the aggregates. While the αSyn aggregates from the PD brain samples were more elongated (fibril-like) than the controls (Figure 4D), Aβ aggregates did not show a difference (Figure 4I), and AT8-positive tau aggregates were more elongated outside the synapse in the AD-brain samples, without a difference between the synaptic aggregates (Figure 4N). Lastly, the synaptosomes from the PD (Figure 4E) and AD (Figure 4J) brain samples on average had greater radius than those from control samples.

Collectively, these results are suggesting that more fibrillar aggregates are present in the PD brain samples, with larger aggregates accumulating in the enlarged synapses in PD,

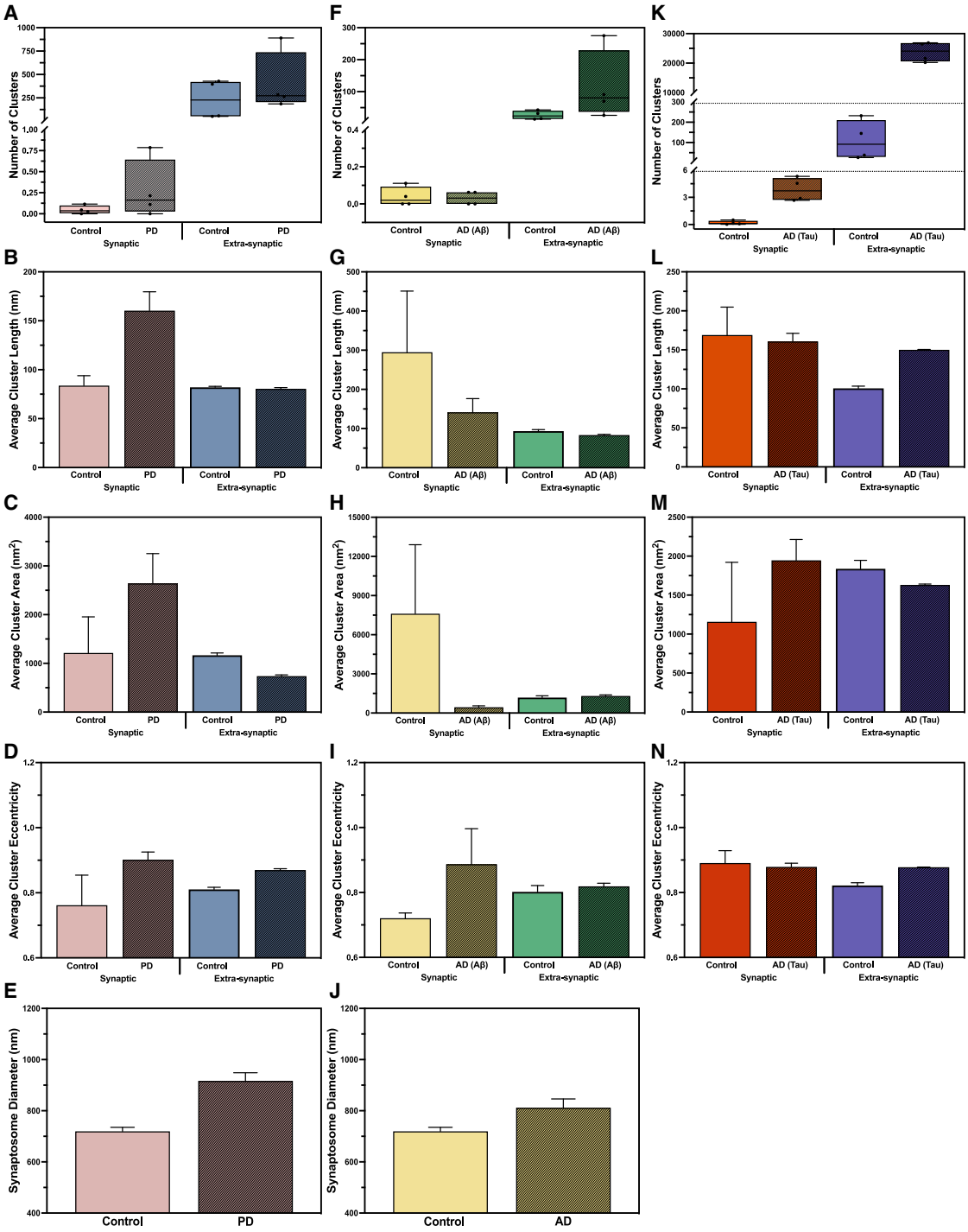

Figure 4. Morphological characteristics of pathological aggregates in human postmortem brain samples

(A, F, and K) Number of synaptic and extra-synaptic aggregates.

(B, G, and L) Average aggregate length in nanometers.

(C, H, and M) Average aggregate area in nanometer square.

(D, I, and N) Average aggregate eccentricity (1 is flat and 0 is circular) for alpha-synuclein, beta-amyloid, and AT8-positive tau aggregates respectively from Parkinson's and Alzheimer's disease, and age-matched control orbitofrontal cortex samples.

(E and J) Average synaptosome diameter.

The analyses were conducted by using data from 124, 94, and 300 synaptosomes harvested from human postmortem orbitofrontal cortex samples from Parkinson's disease, Alzheimer's disease brains, and control samples, respectively and analyzed by linear mixed effects models and 95% confidence intervals. For

(legend continued on next page)

meanwhile the enlarged synapses in AD brains contain smaller Aβ aggregates but a greater number of AT8-positive tau aggregates.

Aggregates in mouse models

Following the postmortem human brain samples, we repeated the same measures in mouse models of PD (MI2[35]), AD (APP^{NL-G-F}[36]), tauopathy (P301S[37]), and wildtype controls (C57Bl6/J) at 6-month of age (see Table S2 for statistical tests). The aggregates formed in the mice were smaller than the human brain samples, with an average length under 100 nm for all species, and there was an overall trend of longer aggregates inside the synapse (see Figure 3 for representative images).

There were prominent parallels between the mouse models and the human brain samples. For instance, the majority of the αSyn, Aβ, and AT8-positive tau aggregates were found in the extra-synaptic fractions in the mouse samples as well. While 22.4% of the synaptosomes from the control brains contained at least one αSyn aggregate, 12.7% of the synaptosomes from the MI2 mouse brains contained one or more aggregates (CI_{95} = −18.43, 37.92). Meanwhile, 35.4% of the synaptosomes from the control brains contained at least one Aβ aggregate and this value was 49.8% for the synaptosomes harvested from the brains of APP^{NL-G-F} mice (CI_{95} = −6.51, 35.40). On the other hand, a significantly higher portion of synaptosomes from the P301S mouse brains contained one or more AT8-positive tau aggregates (38.6%), compared to the ones from the control brains (11.6%; CI_{95} = 3.98, 50.04).

Moreover, the number of αSyn and Aβ aggregates did not differ between the transgenic (MI2 and APP^{NL-G-F}) and wildtype control mouse brains (Figures 5A and 5F), but the P301S mice had significantly more AT8-positive tau aggregates than the controls both in the synaptosomes and the extra-synaptic samples (Figure 5K). While the αSyn aggregates from the MI2 mice were longer than the ones in the control mice (100 nm vs. ∼85 nm), the synaptic αSyn aggregates were longer than the extra-synaptic ones regardless of genotype (∼110 nm vs. 80 nm; Figure 5B). Similarly, the APP^{NL-G-F} mice had longer Aβ aggregates than the controls (∼83 nm vs. 75 nm), but the difference reached statistical significance only for the extra-synaptic aggregates. Meanwhile, the synaptic Aβ aggregates were longer than the extra-synaptic ones, regardless of genotype (∼96 nm vs. 80 nm; Figure 5G). A similar trend was observed for the AT8-positive tau aggregates as well, as the synaptic aggregates were significantly longer than the extra-synaptic ones (∼96 nm vs. 76 nm), regardless of genotype (Figure 5L).

Similar to αSyn aggregate length, the average aggregate area was also larger for the MI2 mice, compared to the controls, yet there was no area difference between the synaptic and extra-synaptic aggregates (Figure 5C). While the area of the synaptic Aβ aggregates did not show a genotype difference, the APP^{NL-G-F} mice had larger aggregates in the extra-synaptic fractions (Figure 5H). On the other hand, the synaptic AT8-positive tau aggregates were significantly larger than the extra-synaptic ones, regardless of genotype (Figure 5M).

The trends for aggregate shape differed considerably between the species; while the extra-synaptic αSyn aggregates from the MI2 mice were more circular than the ones from the control mouse brain (Figure 5D), the Aβ and AT8-positive tau aggregates were more elongated in the brains of the APP^{NL-G-F} (Figure 5I) and P301S mice (Figure 5N) respectively. Lastly, there was no genotype difference between the synaptosomes size from MI2 and P301S mouse brains compared to the controls (Figures 5E and 5O), but the synaptosomes from the APP^{NL-G-F} mice had a greater radius compared to the ones from the control mice (Figure 5J).

The abundance of AT8-positive tau aggregates in human and mouse synaptosomes is also measured in detail. The average number of aggregates per synaptosome is found to be 0.1 and 4.1 in control and AD human samples, respectively, and 0.2 and 0.4 in control and disease mouse samples, respectively. Furthermore, the distribution of aggregate per synaptosome numbers allowed us to perform additional statistical analyses, specifically to investigate if the appearance of each individual aggregate is a random event or if the presence of one aggregate increases the chance of finding another in the same synaptosome. If indeed the appearance of aggregates were random, the distribution of aggregates per synaptosome should follow a Poisson distribution. Based on the fraction of synaptosomes that contain no aggregates, we should then be able to predict the fractions of synaptosomes that have one aggregate, two aggregates, and so on. In Figure 6, we show the experimentally measured distribution (histogram) as well as this prediction (solid gray line). We also show the maximum likelihood, i.e., ''best-fit'', Poisson distribution. A property of this best-fit distribution is that its mean, λ, matches the sample mean. If the data are indeed Poisson distributed, those two distributions would be the same. We find that both mouse datasets (Figures 6C and 6D), as well as the control human dataset (Figure 6A) are Poisson distributed. However, the distribution of aggregates per synaptosome obtained from the human AD samples clearly deviates from the best-fit Poisson distribution (Figure 6B). The two Poisson distributions shown, based on the average number or the fraction of synaptosomes without aggregates, illustrate clearly that there is a significantly higher fraction of synaptosomes with multiple aggregates than would be expected for a random Poisson distributed event. In other words, if a synaptosome has one AT8-positive tau aggregate, it is more likely to have another—than would be expected if the appearance of aggregates were independent events.

DISCUSSION

Synaptic dysfunction is one of the core pathologies seen in AD and PD, promoting cognitive and behavioral deficits.

αSyn, aggregate length, area, and eccentricity, as well as synaptosome radius show significant differences as the synaptic aggregates are longer, larger, and more fibrillar than the extra-synaptic ones. Synaptosomes from PD brains also have a greater diameter than the ones from the control brain. For Aβ, aggregate length and area, as well as synaptosome radius show significant differences as the synaptic aggregates are longer and larger. For AT8-positive tau, both synaptic and extra-synaptic aggregate count is significantly higher in the AD brains compared to the controls. Synaptosomes from AD brains also have a greater diameter than the ones from the control brains.

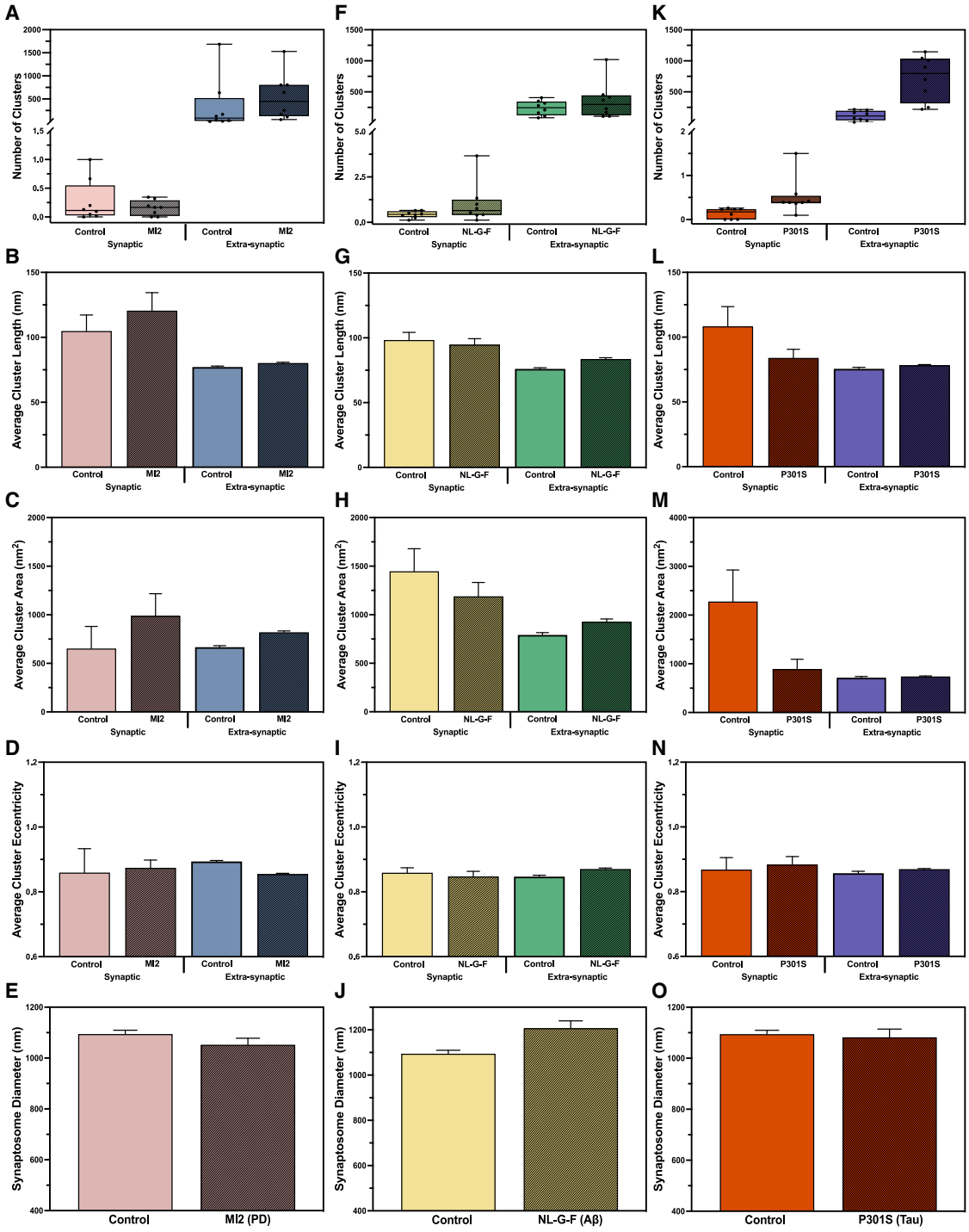

Figure 5. Morphological characteristics of pathological aggregates in MI2, APP^{NL-G-F}, P301S, and C57Bl/6J mouse brain samples

(A, F, and K) Number of synaptic and extra-synaptic aggregates.

(B, G, and L) Average aggregate length in nanometers.

(C, H, and M) Average aggregate area in nanometer square.

(D, I, and N) Average aggregate eccentricity (1 is flat and 0 is circular) for alpha-synuclein, beta-amyloid, and AT8-positive tau aggregates respectively from MI2, APP^{NL-G-F}, P301S, and C57Bl/6J mouse brains.

(E, J, and O) Average synaptosome diameter.

(legend continued on next page)

Interestingly, Aβ, tau, and αSyn all have physiological roles in the synapse, but their pathological aggregation and accumulation causes synaptic dysfunction and loss.[29,38] Our group has been developing single-molecule pull-down (SiMPull) and super-resolution microscopy-based techniques to study pathological aggregates of αSyn, Aβ, and tau in human brain[39] and biofluid[40] samples, as well as model systems.[41] Here, we have developed and described SynPull as a method for characterizing soluble aggregates inside the synapses by combining SiMPull, *d*STORM super-resolution imaging, and advanced computational analysis tools and applied them to postmortem brain samples from AD and PD patients, as well as mouse models.

We used the pre-synaptic protein NRXN1 to reliably capture the synaptosomes. Since the fractured membrane particles can also fuse and form empty liposomes, using a synaptic protein to capture the bassoon-positive synaptosomes enabled us to reliably target the liposomes containing the synaptic compartment (Figure 2D). Then, we used image analysis tools to identify the synaptosomes based on their size, determined by the CellMask signal (Figure 2G). Lastly, we used *d*STORM to super-resolve the aggregates inside and outside the synaptosomes, allowing the morphological characterization of individual soluble aggregates with a resolution-limit of 20 nm. Importantly, these methods are not limited to synaptosomes from human brains and mouse models of neurodegeneration; a broad range of pathologies and/or developmental stages can be reliably studied with high specificity by using appropriate capture antibodies.

Even though the primary aim of this work was to develop a method to study small-soluble aggregates in the synapse, by studying postmortem human disease brain samples and mouse models, we could make biological observations. Regardless of aggregate type, most of the aggregates were extra-synaptic with relatively few synaptosomes containing one or more aggregates (Figure 7). While the least common aggregate type in the synapse was Aβ, AT8-positive tau was the most common aggregate. This observation is interesting since both Aβ and tau aggregates were studied in the same human sample, obtained from the same AD brain, and it is in-line with the findings of Colom-Cadena et al., who found abundant oligomeric tau accumulation in the AD brain, even in regions without robust tau tangle pathology.[16]

The Aβ and αSyn aggregates inside the synaptosomes were larger than the extra-synaptic ones, indicating the presence of a specific population of aggregates accumulating in the synapses. Moreover, the synaptosomes in human brains from the AD and PD patients were larger than those from controls. This has been previously observed in AD brain samples and suggested to reflect a compensatory mechanism against synaptic loss.[42] This observation of potential enlarging of the synapse to make up for synaptic loss also shows a possible limitation of postmortem synaptosome studies: since synaptic loss is common in both AD and PD, the synaptosomes available for harvesting in the postmortem tissue may reflect a survival bias. Interestingly, Zwang et al.,[43] has recently shown that neurons with neurofibrillary tangles have a reduced risk of dying in mouse models of AD. A similar mechanism may exist for synaptic aggregates with tau containing synapses in AD protected, while Aβ containing synapses getting pruned or lost due to other mechanisms.[44]

The presence of Aβ in the synapse and its physiological role has been long studied. While monomeric Aβ at physiological levels seems to be required for synaptic function,[45] oligomeric aggregates disrupt both synapse formation[46] and function.[47] Interestingly, monomeric Aβ has been shown to interact with the soluble oligomeric aggregates and reduce their toxicity.[48] On the other hand, the presence of Aβ has been shown to translocate tau to the synapse.[13] Our results agree with this, as the synaptic AT8-positive tau aggregates were significantly higher in the AD brain. Since the synaptosomes were prepared from the same brain samples for Aβ and tau analyses, our results are also suggesting that tau is significantly more common in the orbito-frontal cortex synapses at later AD stages. Our data modeling also revealed that the presence of AT8-positive tau aggregates in the synapse is not a random event and having one aggregate in the synapse increases the chance of having multiple aggregates (Figures 6 and 7). Mechanistically, there are two possible interpretations of this observation: (1) the appearance of the first aggregate makes the appearance of the second more likely, possibly by self-replication of the first aggregate. (2) A confounding factor means that one subset of synapses contains a much higher average number of aggregates than the other subset. This could be, for example, the subset of synapses that is located close to an Aβ plaque, or the subset of synapses that is connected to cells which contain a tau tangle. The fact that this behavior is only observed in the data from human AD samples but not in those from the P301S mice suggests that Aβ may be an important factor in synaptic AT8-positive tau aggregation, even though Aβ itself does not aggregate in the synapse. Alternatively, it may also be due to the differences in the rate of pathology in humans with AD which takes decades, and the mouse model in which the pathological tau expression begins early in life and is promoter-regulated.

Interestingly, unlike Aβ and αSyn, the synaptic tau aggregates did not differ in size from the extra-synaptic ones. However, it must be noted that all aggregates were harvested by the synaptoneurosome preparation protocol, which only yields a sub-population of the soluble aggregates in the tissue samples. Indeed, the length distribution of tau aggregates in the homogenized AD brain samples were shown to be slightly smaller compared to our previous work, which studied all the soluble AT8-positive tau aggregates harvested through homogenization of the brain tissue.[39] On the other hand, the greatest size difference based on disease condition and synaptic localization was observed in the αSyn aggregates studied in PD brain samples. Similar to Aβ the (patho)physiological role of αSyn in the synapse is

The analyses were conducted by using data from 160, 149, 119, and 520 synaptosomes harvested from MI2, APP^{NL-G-F}, P301S, and C57Bl/6J mouse brains, respectively, and analyzed by linear mixed effects models and 95% confidence intervals.
For αSyn synaptic aggregates are longer than the extra-synaptic ones. For Aβ, synaptosomes from the APP^{NL-G-F} mice are larger than the ones from the control mice. For AT8-positive tau, both synaptic and extra-synaptic aggregate count is significantly higher in the P301S mice than the control mice. The aggregates are also longer, larger, and more fibrillar in the P301S mice.

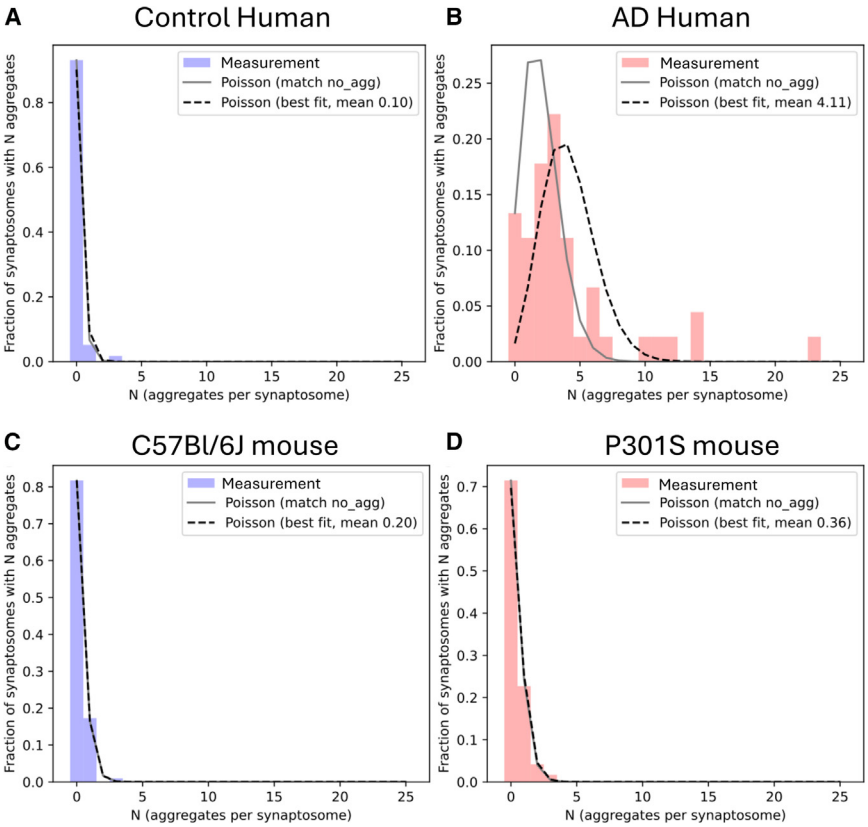

Figure 6. Aggregate per synaptosome distributions from experiment and theory

Experimentally measured aggregate per synaptosome distributions (bars), for (A and B) human and (C and D) mouse samples. The predicted Poisson distribution, based on either matching the fraction of synaptosomes without aggregates (solid gray line) or the average number of aggregates per synaptosome (dashed black line) is shown overlaid. For all except the data from human AD samples (B) the 2 predicted distributions overlap with each other and match the data. For the human AD samples, there are more synaptosomes with higher numbers of aggregates than would be expected based on the total fraction of synaptosomes that contain aggregates (compare bars to solid gray line), indicating that the appearance of individual aggregates are not independent events as in the other 3 datasets.

believed to be determined by its aggregation state: in its native state, αSyn is membrane-bound and interacts with synaptobrevin-2 to facilitate SNARE complex formation and neurotransmitter release.[49] However, when detached from the vesicle membrane, αSyn can start to aggregate, which leads to loss of function as well as gain of toxic function.[38] Lacking a transmembrane domain, αSyn easily dissociates from membranes, which led to the lack of its observation in earlier synaptic isolations.[50] Nevertheless, more recent studies with highly sensitive methods determined the presence of αSyn in synaptosomes as well as synaptic vesicles,[51,52] showing the utility of highly sensitive methods.[53]

In conclusion, here we demonstrated an advanced method to study the morphology of the small-soluble aggregates in synapses, using a specific and selective capturing method, along with super-resolution microscopy, aided by specialized data processing techniques. Using these methods, we have studied Aβ, AT8-positive tau, and αSyn in human brain samples as well as mouse models. We have shown that tau is the most common aggregate type in the synapses in AD brain, meanwhile, even though they are much more rare, Aβ and αSyn aggregates in the synapse are larger than the extra-synaptic ones.

Limitations of the study

While these results are showing the utility of SynPull to study sub-diffraction limit pathological aggregates in synapses, which are invisible to most other imaging techniques, it has some limitations that can be addressed in future work. While synaptosomes are three-dimensional structures, the imaging within the TIRF field is two-dimensional, disabling the exact localization of the aggregates within the synaptosome. Moreover, the relatively low yield of human brain for synaptosomes (Figure 2F) requires manual scanning of the surface to locate and image the synaptic fragments, which is time consuming. Further optimization of the harvesting to enrich for synaptosomes would be beneficial to accelerate the imaging process, by allowing the usage of automated scanning. Lastly, while the results we present here show the utility of SynPull, they need to be further verified in larger sample cohorts, including multiple brain regions and disease stages, as well as different antibodies specific to different Aβ fragments, phosphorylation of tau at other regions, and αSyn with post-translational modifications.

RESOURCE AVAILABILITY

Lead contact

Requests for further information and resources should be directed to Professor Sir David Klenerman, Yusuf Hamied Department of Chemistry, University of Cambridge (dk10012@cam.ac.uk).

Materials availability

This study did not generate new unique reagents.

Data and code availability

- Data availability: Data reported in this paper will be shared by the lead contact upon request.
- Code availability: All original code has been deposited at github and is publicly available as of the date of publication. DOIs are listed in the key resources table.
- Any additional information required to analyze the data reported in this paper is available from the lead contact upon request.

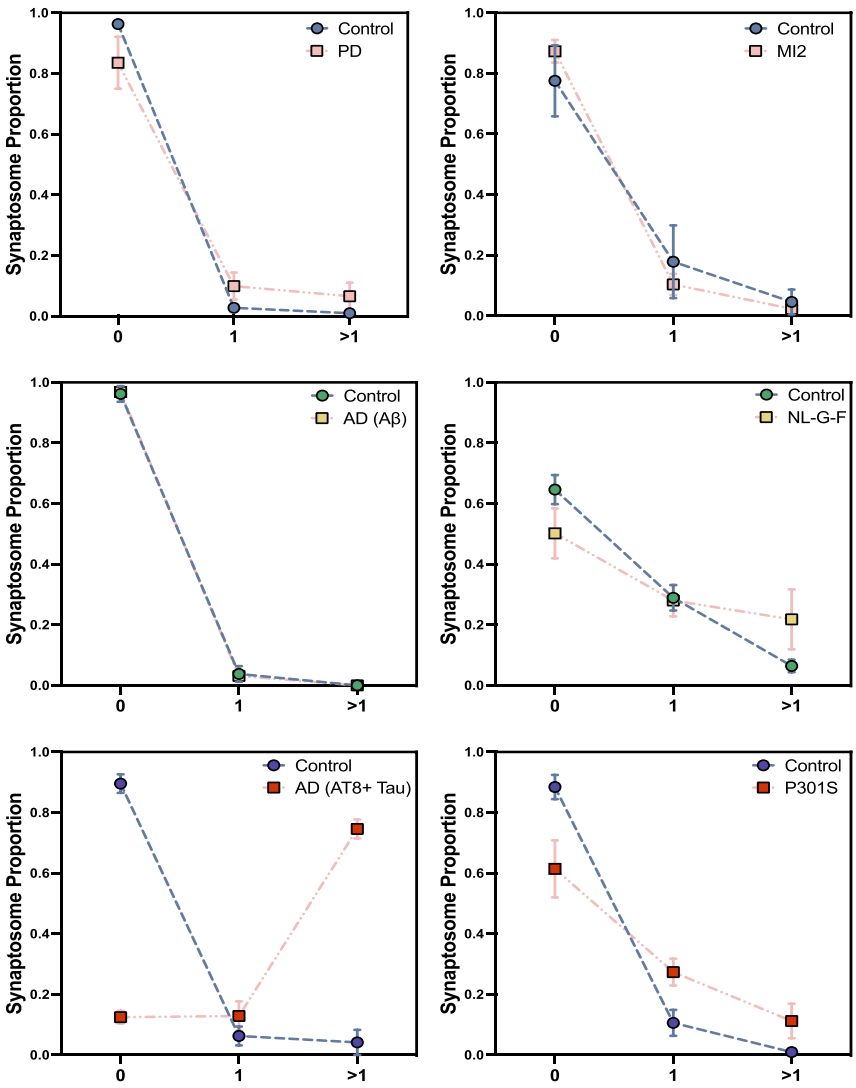

Figure 7. The proportion of synaptosomes with zero, one, and greater than one alpha-synuclein (top row), beta-amyloid (middle row), and AT8-positive tau (bottom row) aggregates from postmortem human (left column) and mouse (right column) brain samples.

ACKNOWLEDGMENTS

We thank Dr. Marc Aurel Busche for providing valuable feedback on the manuscript. EM specimen preparation and TEM were performed using the facilities at CAIC (Cambridge Advanced Imaging Center). We thank Karin Müller, Filomena Gallo, and Georgina Lindop for their kind support and help.

Funding: This work was funded by Parkinson's UK (M.G.S.), UK DRI pilot studies program (J.S.H.D.), and UK Dementia Research Institute through UK DRI Ltd, principally funded by the Medical Research Council (D.K.). D.K. holds a Royal Society Professorship.

AUTHOR CONTRIBUTIONS

S.K.: conception and design, data collection and image analysis, and manuscript preparation. E.F.: conception and design, data collection and statistical analysis, and manuscript writing. G.M.: data modeling. Y.W.: image analysis. Y.P.Z. and J.Y.L.L.: data collection. F.K.W. and W.A.M.: providing the mouse samples. A.Q.: providing human brain samples and neuropathological characterization. M.G.S.: conception and design, providing the mouse samples, and manuscript preparation. J.S.H.D.: conception and design, data collection, and image analysis. D.K.: conception and design, manuscript preparation, and overall supervision of the project.

DECLARATION OF INTERESTS

The authors declare no competing interests.

STAR★METHODS

Detailed methods are provided in the online version of this paper and include the following:

- KEY RESOURCES TABLE
- EXPERIMENTAL MODEL AND STUDY PARTICIPANT DETAILS
- METHOD DETAILS
  - Synaptosome preparation
  - Transmission electron microscopy (TEM)
  - SiMPull coverslip preparation
  - Capturing the synaptosomes on SiMPull
  - Staining the synaptosomes
  - Immunolabeling the synaptic proteins
  - *d*STORM imaging
  - Image processing and analysis
- QUANTIFICATION AND STATISTICAL ANALYSIS

SUPPLEMENTAL INFORMATION

Supplemental information can be found online at https://doi.org/10.1016/j.chembiol.2025.01.001.

Received: September 11, 2024
Revised: November 9, 2024
Accepted: January 3, 2025
Published: January 24, 2025

REFERENCES

1. Busche, M.A., and Hyman, B.T. (2020). Synergy between amyloid-β and tau in Alzheimer's disease. Nat. Neurosci. *23*, 1183–1193. https://doi.org/10.1038/s41593-020-0687-6.
2. De Strooper, B., and Karran, E. (2016). The Cellular Phase of Alzheimer's Disease. Cell *164*, 603–615. https://doi.org/10.1016/j.cell.2015.12.056.
3. Bernal-Conde, L.D., Ramos-Acevedo, R., Reyes-Hernández, M.A., Balbuena-Olvera, A.J., Morales-Moreno, I.D., Argüero-Sánchez, R., Schüle, B., and Guerra-Crespo, M. (2020). Alpha-Synuclein Physiology and Pathology: A Perspective on Cellular Structures and Organelles. Front. Neurosci. *13*, 1399.
4. Spillantini, M.G., Schmidt, M.L., Lee, V.M., Trojanowski, J.Q., Jakes, R., and Goedert, M. (1997). Alpha-synuclein in Lewy bodies. Nature *388*, 839–840. https://doi.org/10.1038/42166.
5. Gcwensa, N.Z., Russell, D.L., Cowell, R.M., and Volpicelli-Daley, L.A. (2021). Molecular Mechanisms Underlying Synaptic and Axon Degeneration in Parkinson's Disease. Front. Cell. Neurosci. *15*, 626128.
6. Tzioras, M., McGeachan, R.I., Durrant, C.S., and Spires-Jones, T.L. (2023). Synaptic degeneration in Alzheimer disease. Nat. Rev. Neurol. *19*, 19–38. https://doi.org/10.1038/s41582-022-00749-z.
7. Griffiths, J., and Grant, S.G.N. (2023). Synapse pathology in Alzheimer's disease. Semin. Cell Dev. Biol. *139*, 13–23. https://doi.org/10.1016/j.semcdb.2022.05.028.
8. Kamenetz, F., Tomita, T., Hsieh, H., Seabrook, G., Borchelt, D., Iwatsubo, T., Sisodia, S., and Malinow, R. (2003). APP Processing and Synaptic Function. Neuron *37*, 925–937. https://doi.org/10.1016/S0896-6273(03)00124-7.
9. Plant, L.D., Boyle, J.P., Smith, I.F., Peers, C., and Pearson, H.A. (2003). The production of amyloid β peptide is a critical requirement for the viability of central neurons. J. Neurosci. *23*, 5531–5535. https://doi.org/10.1523/jneurosci.23-13-05531.2003.
10. Sharma, M., Burré, J., and Südhof, T.C. (2012). Proteasome inhibition alleviates SNARE-dependent neurodegeneration. Sci. Transl. Med. *4*, 147ra113. https://doi.org/10.1126/scitranslmed.3004028.
11. Yang, Y., Kim, J., Kim, H.Y., Ryoo, N., Lee, S., Kim, Y., Rhim, H., and Shin, Y.K. (2015). Amyloid-β Oligomers May Impair SNARE-Mediated Exocytosis by Direct Binding to Syntaxin 1a. Cell Rep. *12*, 1244–1251. https://doi.org/10.1016/j.celrep.2015.07.044.
12. Dinamarca, M.C., Weinstein, D., Monasterio, O., and Inestrosa, N.C. (2011). The synaptic protein neuroligin-1 interacts with the amyloid β-peptide. is there a role in Alzheimer's disease? Biochemistry *50*, 8127–8137. https://doi.org/10.1021/bi201246t.
13. Frandemiche, M.L., Seranno, S.D., Rush, T., Borel, E., Elie, A., Arnal, I., Lanté, F., and Buisson, A. (2014). Activity-dependent tau protein translocation to excitatory synapse is disrupted by exposure to amyloid-beta oligomers. J. Neurosci. *34*, 6084–6097. https://doi.org/10.1523/JNEUROSCI.4261-13.2014.
14. Zhou, L., McInnes, J., Wierda, K., Holt, M., Herrmann, A.G., Jackson, R.J., Wang, Y.C., Swerts, J., Beyens, J., Miskiewicz, K., et al. (2017). Tau association with synaptic vesicles causes presynaptic dysfunction. Nat. Commun. *8*, 15295. https://doi.org/10.1038/ncomms15295.
15. Robbins, M., Clayton, E., and Kaminski Schierle, G.S. (2021). Synaptic tau: A pathological or physiological phenomenon? Acta Neuropathol. Commun. *9*, 149. https://doi.org/10.1186/s40478-021-01246-y.
16. Colom-Cadena, M., Davies, C., Sirisi, S., Lee, J.-E., Simzer, E.M., Tzioras, M., Querol-Vilaseca, M., Sánchez-Aced, É., Chang, Y.Y., Holt, K., et al. (2023). Synaptic oligomeric tau in Alzheimer's disease - A potential culprit in the spread of tau pathology through the brain. Neuron *111*, 2170–2183.e6. https://doi.org/10.1016/j.neuron.2023.04.020.
17. Diao, J., Burré, J., Vivona, S., Cipriano, D.J., Sharma, M., Kyoung, M., Südhof, T.C., and Brunger, A.T. (2013). Native α-synuclein induces clustering of synaptic-vesicle mimics via binding to phospholipids and synaptobrevin-2/VAMP2. Elife *2*, e00592. https://doi.org/10.7554/eLife.00592.
18. Garcia-Reitböck, P., Anichtchik, O., Bellucci, A., Iovino, M., Ballini, C., Fineberg, E., Ghetti, B., Della Corte, L., Spano, P., Tofaris, G.K., et al. (2010). SNARE protein redistribution and synaptic failure in a transgenic mouse model of Parkinson's disease. Brain *133*, 2032–2044. https://doi.org/10.1093/brain/awq132.
19. Choi, B.K., Choi, M.G., Kim, J.Y., Yang, Y., Lai, Y., Kweon, D.H., Lee, N.K., and Shin, Y.K. (2013). Large α-synuclein oligomers inhibit neuronal SNARE-mediated vesicle docking. Proc. Natl. Acad. Sci. USA *110*, 4087–4092. https://doi.org/10.1073/pnas.1218424110.
20. Yoo, G., Yeou, S., Son, J.B., Shin, Y.-K., and Lee, N.K. (2021). Cooperative inhibition of SNARE-mediated vesicle fusion by α-synuclein monomers and oligomers. Sci. Rep. *11*, 10955. https://doi.org/10.1038/s41598-021-90503-0.
21. Ingelsson, M. (2016). Alpha-Synuclein Oligomers-Neurotoxic Molecules in Parkinson's Disease and Other Lewy Body Disorders. Front. Neurosci. *10*, 408. https://doi.org/10.3389/FNINS.2016.00408.
22. Emin, D., Zhang, Y.P., Lobanova, E., Miller, A., Li, X., Xia, Z., Dakin, H., Sideris, D.I., Lam, J.Y.L., Ranasinghe, R.T., et al. (2022). Small soluble α-synuclein aggregates are the toxic species in Parkinson's disease. Nat. Commun. *13*, 5512. https://doi.org/10.1038/s41467-022-33252-6.
23. Danial, J.S.H., and Klenerman, D. (2021). Single molecule imaging of protein aggregation in Dementia: Methods, insights and prospects. Neurobiol. Dis. *153*, 105327. https://doi.org/10.1016/j.nbd.2021.105327.
24. Villasana, L.E., Klann, E., and Tejada-Simon, M.V. (2006). Rapid isolation of synaptoneurosomes and postsynaptic densities from adult mouse hippocampus. J. Neurosci. Methods *158*, 30–36. https://doi.org/10.1016/j.jneumeth.2006.05.008.
25. Hebb, C.O., and Whittaker, V.P. (1958). Intracellular distributions of acetylcholine and choline acetylase. J. Physiol. *142*, 187–196. https://doi.org/10.1113/jphysiol.1958.sp006008.
26. Dashkova, A.S., Kovalev, V.I., Chaplygina, A.V., Zhdanova, D.Y., and Bobkova, N.V. (2024). Unique Properties of Synaptosomes and Prospects for Their Use for the Treatment of Alzheimer's Disease. Biochemistry *89*, 1031–1044. https://doi.org/10.1134/S0006297924060051.
27. Postupna, N.O., Latimer, C.S., Keene, C.D., Montine, K.S., Montine, T.J., and Darvas, M. (2018). Flow cytometric evaluation of crude synaptosome preparation as a way to study synaptic alteration in neurodegenerative diseases. Neuromethods *141*, 297–310. https://doi.org/10.1007/978-1-4939-8739-9_17.
28. Jhou, J.-F., and Tai, H.-C. (2017). The Study of Postmortem Human Synaptosomes for Understanding Alzheimer's Disease and Other Neurological Disorders: A Review. Neurol. Ther. *6*, 57–68. https://doi.org/10.1007/s40120-017-0070-z.
29. Spires-Jones, T.L., and Hyman, B.T. (2014). The intersection of amyloid beta and tau at synapses in Alzheimer's disease. Neuron *82*, 756–771. https://doi.org/10.1016/J.NEURON.2014.05.004.
30. Henstridge, C.M., Pickett, E., and Spires-Jones, T.L. (2016). Synaptic pathology: A shared mechanism in neurological disease. Ageing Res. Rev. *28*, 72–84. https://doi.org/10.1016/j.arr.2016.04.005.
31. Cai, Q., and Tai, H.-C. (2024). Super-Resolution Imaging of Tau Proteins in Isolated and Immobilized Brain Synaptosomes. Methods Mol. Biol. *2754*, 445–456. https://doi.org/10.1007/978-1-0716-3629-9_24.
32. Chen, J., Yu, S., Fu, Y., and Li, X. (2014). Synaptic proteins and receptors defects in autism spectrum disorders. Front. Cell. Neurosci. *8*, 276. https://doi.org/10.3389/fncel.2014.00276.

33. O'Brien, S.F., and Yi, Q.L. (2016). How do I interpret a confidence interval? Transfusion *56*, 1680–1683. https://doi.org/10.1111/trf.13635.

34. Pascu, A., Romanitan, M.O., Delgado, J.-M., Danaila, L., and Pascu, M.L. (2009). Laser-Induced Autofluorescence Measurements on Brain Tissues. Anat. Rec. *292*, 2013–2022. https://doi.org/10.1002/ar.21034.

35. Wegrzynowicz, M., Bar-On, D., Calo', L., Anichtchik, O., Iovino, M., Xia, J., Ryazanov, S., Leonov, A., Giese, A., Dalley, J.W., et al. (2019). Depopulation of dense α-synuclein aggregates is associated with rescue of dopamine neuron dysfunction and death in a new Parkinson's disease model. Acta Neuropathol. *138*, 575–595. https://doi.org/10.1007/s00401-019-02023-x.

36. Nilsson, P., Saito, T., and Saido, T.C. (2014). New mouse model of Alzheimer's. ACS Chem. Neurosci. *5*, 499–502. https://doi.org/10.1021/cn500105p.

37. Allen, B., Ingram, E., Takao, M., Smith, M.J., Jakes, R., Virdee, K., Yoshida, H., Holzer, M., Craxton, M., Emson, P.C., et al. (2002). Abundant tau filaments and nonapoptotic neurodegeneration in transgenic mice expressing human P301S tau protein. J. Neurosci. *22*, 9340–9351. https://doi.org/10.1523/JNEUROSCI.22-21-09340.2002.

38. Gao, V., Briano, J.A., Komer, L.E., and Burré, J. (2023). Functional and Pathological Effects of α-Synuclein on Synaptic SNARE Complexes. J. Mol. Biol. *435*, 167714. https://doi.org/10.1016/j.jmb.2022.167714.

39. Böken, D., Cox, D., Burke, M., Lam, J.Y.L., Katsinelos, T., Danial, J.S.H., Fertan, E., McEwan, W.A., Rowe, J.B., and Klenerman, D. (2024). Single-Molecule Characterization and Super-Resolution Imaging of Alzheimer's Disease-Relevant Tau Aggregates in Human Samples. Angew. Chem., Int. Ed. Engl. *63*, e202317756. https://doi.org/10.1002/anie.202317756.

40. Lobanova, E., Whiten, D., Ruggeri, F.S., Taylor, C.G., Kouli, A., Xia, Z., Emin, D., Zhang, Y.P., Lam, J.Y.L., Williams-Gray, C.H., and Klenerman, D. (2022). Imaging protein aggregates in the serum and cerebrospinal fluid in Parkinson's disease. Brain *145*, 632–643. https://doi.org/10.1093/brain/awab306.

41. Fertan, E., Böken, D., Murray, A., Danial, J.S.H., Lam, J.Y.L., Wu, Y., Goh, P.A., Alić, I., Cheetham, M.R., Lobanova, E., et al. (2023). Cerebral organoids with chromosome 21 trisomy secrete Alzheimer's disease-related soluble aggregates detectable by single-molecule-fluorescence and super-resolution microscopy. Mol. Psychiatr. *29*, 369–386. https://doi.org/10.1038/s41380-023-02333-3.

42. Bhembre, N., Bonthron, C., and Opazo, P. (2023). Synaptic Compensatory Plasticity in Alzheimer's Disease. J. Neurosci. *43*, 6833–6840. https://doi.org/10.1523/JNEUROSCI.0379-23.2023.

43. Zwang, T.J., Sastre, E.D., Wolf, N., Ruiz-Uribe, N., Woost, B., Hoglund, Z., Fan, Z., Bailey, J., Nfor, L., Buée, L., et al. (2024). Neurofibrillary tangle-bearing neurons have reduced risk of cell death in mice with Alzheimer's pathology. Cell Rep. *43*, 114574. https://doi.org/10.1016/j.celrep.2024.114574.

44. Qu, J., Nakamura, T., Cao, G., Holland, E.A., McKercher, S.R., and Lipton, S.A. (2011). S-Nitrosylation activates Cdk5 and contributes to synaptic spine loss induced by beta-amyloid peptide. Proc. Natl. Acad. Sci. USA *108*, 14330–14335. https://doi.org/10.1073/pnas.1105172108.

45. Zhou, B., Lu, J.G., Siddu, A., Wernig, M., and Südhof, T.C. (2022). Synaptogenic effect of APP-Swedish mutation in familial Alzheimer's disease. Sci. Transl. Med. *14*, eabn9380. https://doi.org/10.1126/scitranslmed.abn9380.

46. Naito, Y., Tanabe, Y., Lee, A.K., Hamel, E., and Takahashi, H. (2017). Amyloid-β Oligomers Interact with Neurexin and Diminish Neurexin-mediated Excitatory Presynaptic Organization. Sci. Rep. *7*, 42548. https://doi.org/10.1038/srep42548.

47. He, Y., Wei, M., Wu, Y., Qin, H., Li, W., Ma, X., Cheng, J., Ren, J., Shen, Y., Chen, Z., et al. (2019). Amyloid β oligomers suppress excitatory transmitter release via presynaptic depletion of phosphatidylinositol-4,5-bisphosphate. Nat. Commun. *10*, 1193. https://doi.org/10.1038/s41467-019-09114-z.

48. Bate, C., and Williams, A. (2018). Monomeric amyloid-β reduced amyloid-β oligomer-induced synapse damage in neuronal cultures. Neurobiol. Dis. *111*, 48–58. https://doi.org/10.1016/j.nbd.2017.12.007.

49. Burré, J., Sharma, M., Tsetsenis, T., Buchman, V., Etherton, M.R., and Südhof, T.C. (2010). Alpha-synuclein promotes SNARE-complex assembly *in vivo* and *in vitro*. Science *329*, 1663–1667. https://doi.org/10.1126/science.1195227.

50. Takamori, S., Holt, M., Stenius, K., Lemke, E.A., Grønborg, M., Riedel, D., Urlaub, H., Schenck, S., Brügger, B., Ringler, P., et al. (2006). Molecular anatomy of a trafficking organelle. Cell *127*, 831–846. https://doi.org/10.1016/j.cell.2006.10.030.

51. Taoufiq, Z., Ninov, M., Villar-Briones, A., Wang, H.-Y., Sasaki, T., Roy, M.C., Beauchain, F., Mori, Y., Yoshida, T., Takamori, S., et al. (2020). Hidden proteome of synaptic vesicles in the mammalian brain. Proc. Natl. Acad. Sci. USA *117*, 33586–33596. https://doi.org/10.1073/pnas.2011870117.

52. Caló, L., Hidari, E., Wegrzynowicz, M., Dalley, J.W., Schneider, B.L., Podgajna, M., Anichtchik, O., Carlson, E., Klenerman, D., and Spillantini, M.G. (2021). CSPα reduces aggregates and rescues striatal dopamine release in α-synuclein transgenic mice. Brain *144*, 1661–1669. https://doi.org/10.1093/brain/awab076.

53. Lautenschläger, J., Stephens, A.D., Fusco, G., Ströhl, F., Curry, N., Zacharopoulou, M., Michel, C.H., Laine, R., Nespovitaya, N., Fantham, M., et al. (2018). C-terminal calcium binding of α-synuclein modulates synaptic vesicle interaction. Nat. Commun. *9*, 712. https://doi.org/10.1038/s41467-018-03111-4.

54. Xia, Z., Wu, Y., Lam, J.Y.L., Zhang, Z., Burke, M., Fertan, E., Ranasinghe, R.T., Hidari, E., Danial, J.S.H., and Klenerman, D. (2023). A computational suite for the structural and functional characterization of amyloid aggregates. Cell Rep. Methods *3*, 100499. https://doi.org/10.1016/J.CRMETH.2023.100499.

55. Ovesný, M., Křížek, P., Borkovec, J., Švindrych, Z., and Hagen, G.M. (2014). ThunderSTORM: a comprehensive ImageJ plug-in for PALM and STORM data analysis and super-resolution imaging. Bioinformatics *30*, 2389–2390. https://doi.org/10.1093/bioinformatics/btu202.

56. Lemke, O., and Keller, B.G. (2016). Density-based cluster algorithms for the identification of core sets. J. Chem. Phys. *145*, 164104. https://doi.org/10.1063/1.4965440.

57. Zhang, Y.P., Lobanova, E., Dworkin, A., Furlepa, M., Yang, W.S., Burke, M., Meng, J.X., Potter, N., Sala, R.L., Kahanawita, L., et al. (2024). Improved Imaging Surface for Quantitative Single-Molecule Microscopy. ACS Appl. Mater. Interfaces *16*, 37255–37264. https://doi.org/10.1021/acsami.4c06512.

58. Danial, J.S.H., Lam, J.Y.L., Wu, Y., Woolley, M., Dimou, E., Cheetham, M.R., Emin, D., and Klenerman, D. (2022). Constructing a cost-efficient, high-throughput and high-quality single-molecule localization microscope for super-resolution imaging. Nat. Protoc. *17*, 2570–2619. https://doi.org/10.1038/S41596-022-00730-6.

59. Braak, H., Del Tredici, K., Rüb, U., de Vos, R.A.I., Jansen Steur, E.N.H., and Braak, E. (2003). Staging of brain pathology related to sporadic Parkinson's disease. Neurobiol. Aging *24*, 197–211. https://doi.org/10.1016/S0197-4580(02)00065-9.

60. Braak, H., and Braak, E. (1991). Neuropathological stageing of Alzheimer-related changes. Acta Neuropathol. *82*, 239–259. https://doi.org/10.1007/BF00308809.

61. du Plessis, S., Bossert, M., Vink, M., van den Heuvel, L., Bardien, S., Emsley, R., Buckle, C., Seedat, S., and Carr, J. (2018). Reward processing dysfunction in ventral striatum and orbitofrontal cortex in Parkinson's disease. Parkinsonism Relat. Disorders *48*, 82–88. https://doi.org/10.1016/j.parkreldis.2017.12.024.

62. Kobayakawa, M., Tsuruya, N., and Kawamura, M. (2017). Decision-making performance in Parkinson's disease correlates with lateral orbitofrontal volume. J. Neurol. Sci. *372*, 232–238. https://doi.org/10.1016/j.jns.2016.11.046.

63. Van Hoesen, G.W., Parvizi, J., and Chu, C.-C. (2000). Orbitofrontal Cortex Pathology in Alzheimer's Disease. Cerebr. Cortex *10*, 243–251. https://doi.org/10.1093/cercor/10.3.243.

64. Scattoni, M.L., Gasparini, L., Alleva, E., Goedert, M., Calamandrei, G., and Spillantini, M.G. (2010). Early behavioural markers of disease in P301S tau transgenic mice. Behav. Brain Res. *208*, 250–257. https://doi.org/10.1016/j.bbr.2009.12.002.

65. Hesse, R., Hurtado, M.L., Jackson, R.J., Eaton, S.L., Herrmann, A.G., Colom-Cadena, M., Tzioras, M., King, D., Rose, J., Tulloch, J., et al. (2019). Comparative profiling of the synaptic proteome from Alzheimer's disease patients with focus on the APOE genotype. Acta Neuropathol. Commun. *7*, 214. https://doi.org/10.1186/s40478-019-0847-7.

66. Richter, K., Langnaese, K., Kreutz, M.R., Olias, G., Zhai, R., Scheich, H., Garner, C.C., and Gundelfinger, E.D. (1999). Presynaptic cytomatrix protein bassoon is localized at both excitatory and inhibitory synapses of rat brain. J. Comp. Neurol. *408*, 437–448. https://doi.org/10.1002/(sici)1096-9861(19990607)408:3<437::aid-cne9>3.0.co.

67. Kedia, S., Ramakrishna, P., Netrakanti, P.R., Jose, M., Sibarita, J.-B., Nadkarni, S., and Nair, D. (2020). Real-time nanoscale organization of amyloid precursor protein. Nanoscale *12*, 8200–8215. https://doi.org/10.1039/d0nr00052c.

68. Kedia, S., Ramakrishna, P., Netrakanti, P.R., Singh, N., Sisodia, S.S., Jose, M., Kumar, S., Mahadevan, A., Ramanan, N., Nadkarni, S., and Nair, D. (2021). Alteration in synaptic nanoscale organization dictates amyloidogenic processing in Alzheimer's disease. iScience *24*, 101924. https://doi.org/10.1016/j.isci.2020.101924.

69. Kedia, S., Ramanan, N., and Nair, D. (2021). Quantifying molecular aggregation by super resolution microscopy within an excitatory synapse from mouse hippocampal neurons. STAR Protoc. *2*, 100470. https://doi.org/10.1016/j.xpro.2021.100470.

70. Belapurkar, V., Mahadeva Swamy, H.S., Singh, N., Kedia, S., Setty, S.R.G., Jose, M., and Nair, D. (2023). Real-time heterogeneity of supramolecular assembly of amyloid precursor protein is modulated by an endocytic risk factor PICALM. Cell. Mol. Life Sci. *80*, 295. https://doi.org/10.1007/s00018-023-04939-w.

71. Mascha, E.J., and Vetter, T.R. (2018). Significance, Errors, Power, and Sample Size: The Blocking and Tackling of Statistics. Anesth. Analg. *126*, 691–698. https://doi.org/10.1213/ANE.0000000000002741.

72. Lumley, T., Diehr, P., Emerson, S., and Chen, L. (2002). The importance of the normality assumption in large public health data sets. Annu. Rev. Publ. Health *23*, 151–169. https://doi.org/10.1146/annurev.publhealth.23.100901.140546.

STAR★METHODS

KEY RESOURCES TABLE

REAGENT or RESOURCE	SOURCE	IDENTIFIER
Antibodies		
Rabbit Polyclonal anti-Neurexin I beta	Abcam	Cat#ab222806; RRID: AB_3665286
Mouse Monoclonal anti-Bassoon/BSN	Abcam	Cat#ab82958; RRID: AB_1860018
Rabbit Polyclonal anti-PSD95	Abcam	Cat#ab18258; RRID: AB_444362
Mouse Monoclonal anti-alpha Synuclein	Thermo Fisher Scientific	Cat#MA1-90346; RRID: AB_1954821
Mouse Monoclonal Biotin (azide-free) anti-β-Amyloid, 1-16	BioLegend	Cat#9340-02; RRID: AB_2564657
Mouse Monoclonal anti-Phospho-Tau (Ser202, Thr205), Biotin	Invitrogen	Cat#MN1020B; RRID: AB_223648
Biological samples		
Healthy human post-mortem orbitofrontal cortex brain tissue	Cambridge Brain Bank (Cambridge University Hospitals), Cambridge, United Kingdom	N/A
Parkinson's disease human post-mortem orbitofrontal cortex brain tissue	Cambridge Brain Bank (Cambridge University Hospitals), Cambridge, United Kingdom	N/A
Alzheimers' disease human post-mortem orbitofrontal cortex brain tissue	Cambridge Brain Bank (Cambridge University Hospitals), Cambridge, United Kingdom	N/A
Chemicals, peptides, and recombinant proteins		
Pluronic F-127™ polymer	Biotium	Cat#59005
CellMask™ plasma membrane stain	Thermo Fischer Scientific	Cat#C10045
Pierce™ 16% Formaldehyde methanol-free	Thermo Fischer Scientific	Cat#28906
Triton-X	Sigma-Aldrich	Cat#X100-5ML
Alexa Fluor™ 488 NHS Ester (Succinimidyl Ester)	Thermo Fischer Scientific	Cat#A20000
Alexa Fluor™ 647 NHS Ester (Succinimidyl Ester)	Thermo Fischer Scientific	Cat#A37573
TetraSpeck fluorescent spheres	Thermo Fischer Scientific	Cat#T7279
Experimental models: Organisms/strains		
Mouse: MI2	Wegrzynowicz et al.[35]	N/A
Mouse: APP^{NL-G-F}	Nilsson et al.[36]	N/A
Mouse: P301S	Allen et al.[37]	RRID:MGI:5450673
Mouse: C57Bl/6J	Charles River Laboratories	RRID:MGI:3028467
Software and algorithms		
Aggregate Characterisation Tool (ACT)	Xia et al.[54]	N/A
ThunderSTORM	Ovesný et al.[55]	https://zitmen.github.io/thunderstorm/
Density-based clustering algorithm (DSBCAN)	Lemke et al.[56]	N/A
R Project Statistical Computing v4.2.2 (2022-10-31)	r-project	https://www.r-project.org/
ImageJ (Fiji)	ImageJ	https://imagej.net/
GraphPad Prism v7.0	GraphPad	https://www.graphpad.com/features
MetaMorph v7.10.5.476	Molecular Devices	https://www.moleculardevices.com/
SynPull Code	This study	https://doi.org/10.5281/zenodo.14444305, https://github.com/jdanial/SynPull
Other		
Dounce homogeniser	Cambridge Scientific	Cat#40401
80 μm nylon filter	Millipore	Cat#NY8002500

(*Continued on next page*)

Continued

REAGENT or RESOURCE	SOURCE	IDENTIFIER
25 mm filter holder	PALL	Cat#4320
5 μm filter	Millipore	Cat#SMWP04700
SiMPull coverslips	Zhang et al.[57]	N/A
Single molecule localisation microscope (NanoPro)	Danial et al.[58]	N/A

EXPERIMENTAL MODEL AND STUDY PARTICIPANT DETAILS

3 PD, 3 AD, and 3 age- and sex-matched (two female, one male) post-mortem human orbitofrontal cortex (Brodmann areas 10-11) samples were acquired from the Cambridge Brain Bank (Cambridge University Hospitals), which is supported by the NIHR Cambridge Biomedical Research Centre (NIHR203312). The average age of death of the donors was 80 ± 6 (PD), 79 ± 6 (AD), and 74 ± 7 (control). The human disease brain samples were selected from Lewy body Braak stages 4/5 for PD[59] and neurofibrillary tangle Braak stages 5/6 for AD.[60] Due to the extensive dopaminergic input to this region from the midbrain, the orbitofrontal cortex is involved in the decision making and reward processing deficits seen in PD.[61,62] Similarly, extensive neurofibrillary tangle pathology is observed in the orbitofrontal cortex of AD patients, especially in Layers 3 and 5.[63] The brain samples were voluntarily donated without any compensation. We gratefully acknowledge the participation of all our patient and control volunteers. Tissue segments were dissected and flash-frozen to be stored in -80°C freezers until further processing.

The disease model mice from which the brain samples were collected were bred in-house at University of Cambridge (MI2 and P301S) and University College London (APPNL-G-F) in accordance with the Animals (Scientific Procedures) Act 1986 (United Kingdom), after local institutional ethical review by the Medical Research Council and in accordance with ARRIVE guidelines. Until tissue collection, same sex mice were housed in individually ventilated cages (Techniplast) with grade 5, autoclaved dust-free wood bedding, paper bedding, and a translucent red "mouse house" in groups of 2-4, with ad-libitum access to food and water. Mice were moved to new cages with fresh bedding once a week. The animal facility was maintained at a constant temperature of 19–23°C with 55 ± 10% humidity in a 12 h light/dark cycle. The C57Bl6/J control mouse brains were purchased from Charles River, UK (Margate, Kent).

The MI2 mice express truncated 1-120 αSyn under the control of the tyrosine hydroxylase promoter in the C57Bl/Ola background without any endogenous αSyn expression, resulting in the selective expression of aggregation-prone C-terminal truncated αSyn in dopaminergic neurons, associated with synaptic aggregation and dysfunction.[35] Three homozygous, 6-month-old, male mice were used in this study, an age which dopaminergic neuronal dysfunction is observed. Due to the anatomically limited expression of the transgene to the dopaminergic neurons, brains were sliced into two parts, separating the midbrain and the dorsal striatum from the rest of the cerebrum.

The APP^{NL-G-F} mice express human amyloid precursor protein (APP) with the Arctic, Swedish, and Iberian mutations under the murine APP promoter and show plaque pathology starting at 2 months of age, which increases up to 7 months of age.[36] Synaptic loss along with cognitive impairment has been observed in this model by 6-months of age.[36] Three homozygous, 6-month-old, male mice were used in this study.

The P301S mice express human 4R/0N tau with the P301S mutation under the neuronal portion of the murine Thy1 promoter, resulting in tau tangle pathology, neuronal loss, and behavioural deficits by 4-months of age.[37,64] Three male mice at 6-months of age were used in this study.

METHOD DETAILS

Synaptosome preparation

The synapto(neuro)some preparation method developed by Tara Spires-Jones and colleagues[65] was used in these experiments. In brief, a full mouse cerebrum (or human tissue of similar size of 300-400 mg) was initially homogenised with 1 mL, ice-cold homogenisation buffer, containing 25 mM HEPES (pH 7.5), 120 mM NaCl, 5 mM KCl, 1 mM MgCl2, and 2 mM CaCl2, dissolved in HPLC-grade water, using a 2 mL Dounce homogeniser (Cambridge Scientific, Cat. 40401). Then the homogenate was first filtered through an 80 μm nylon filter (Millipore, Cat. NY8002500; 25 mm filter holder: PALL, Cat. 4320) to remove tissue debris, followed by a second filtration with a 5 μm filter (Millipore, Cat. SMWP04700), to remove the organelles and the nuclei. Then the homogenate was collected in a 1.5 ml Lo-bind Eppendorf and centrifuged at 1000 g for 5 minutes at 4°C. Because this preparation yields synaptic fragments containing the complete pre-synapse as well as parts of the post-synaptic compartment, the synaptic fragments prepared using this method are termed synaptoneurosomes.[24,65] A total of 1466 synaptosomes (124 from PD, 94 from AD, 300 from control human brain samples along with 160 from MI2, 149 from APP^{NL-G-F}, 119 from P301S, and 520 from C57Bl/6J control mice) were harvested and studied.

Transmission electron microscopy (TEM)

Samples were fixed with a mixture containing 2% glutaraldehyde and 2% formaldehyde in 0.05 M sodium cacodylate buffer (pH 7.4) containing 2 mM $CaCl_2$ overnight at 4°C. After the fixation, samples were washed five times with 0.05 M sodium cacodylate buffer

(pH 7.4) and osmicated in 1% osmium tetroxide and 1.5% potassium ferricyanide in 0.05 M sodium cacodylate buffer (pH 7.4) and osmicated in 1% osmium tetroxide and 1.5% potassium ferricyanide in 0.1 M sodium cacodylate buffer (pH 7.4) for 3 days at 4°C. All samples were then washed five times in deionized water (DIW) and treated with 0.1 % (w/v) thiocarbohydrazide in DIW for 20 minutes at room temperature in the dark. After washing five times with DIW, samples were osmicated a second time for 1 hour at room temperature (2% osmium tetroxide in DIW). After washing five times with DIW, samples were block stained with uranyl acetate (2% uranyl acetate in 0.05 M maleate buffer -pH 5.5) for 3 days at 4°C. Samples were washed five times in DIW and then dehydrated in a graded series of ethanol (50%, 70%, 95%, 100%, 100% dry) and 100% dry acetonitrile, three time in each for at least 5 minutes. Samples were infiltrated with a 50/50 mixture of 100% dry acetonitrile/Quetol resin (without BDMA) overnight, followed by 3 days in 100% Quetol (without BDMA). Then, samples were infiltrated for 5 days in 100% Quetol resin with BDMA, exchanging the resin each day. The Quetol resin mixture is: 12 g Quetol 651, 15.7 g NSA, 5.7 g MNA and 0.5 g BDMA (all from TAAB). Samples were placed in embedding moulds and cured at 60°C for 3 days.

90 nm thick TEM sections were cut by an ultramicrotome (Leica Ultracut) and placed on 300 mesh bare copper grids. Samples were imaged in a Tecnai G2 TEM (FEI/ThermoFisher) run at 200 keV accelerating voltage using a 20 μm objective aperture to improve contrast; images were acquired using an AMT digital camera.

SiMPull coverslip preparation

The SiMPull coverslips were prepared as previously described.[57] In brief, glass coverslips were first cleaned with argon plasma and then coated with a 1:1 mixture of Rain-X liquid and isopropanol. Once the mixture was fully evaporated, the slides were stored in a dark cabinet at room temperature.

Capturing the synaptosomes on SiMPull

SiMPull coverslips were stored in a dark and dry environment in room temperature until used. First, the wells were washed twice with phosphate buffered saline (PBS). Then, neutravidin dissolved in PBS at 0.2 mg/ml was incubated for 10 minutes, followed by two more PBS washes. Next, a Pluronic F-127™ polymer (Biotium, Cat. 59005) dissolved in PBS (1:10 by volume and with 0.2μm filtering) was incubated on the surface for 90 minutes, followed by two washes with PBS with 0.05% Tween (PBST). A biotinylated polyclonal anti-neurexin 1 (NRXN1) antibody (abcam, Cat. ab222806) at 10 nm concentration (in PBST) was added to the surface for 10-minutes, followed by two washes with PBST. Finally, 10 μL of synaptosome sample was added to the surface and incubated overnight at 4°C.

Staining the synaptosomes

An orange CellMask™ plasma membrane stain (Thermo Fischer Scientific, Cat. C10045) was used to label the synaptosomes. Following the overnight incubation of the samples, the surface was washed twice with PBST and a CellMask solution (1:6000 by volume in PBS) was added to the surface for 10 minutes, followed by four rounds of washes with PBS.

Immunolabeling the synaptic proteins

In order to study pre- and post-synaptic marker proteins, as well as Aβ aggregates inside the synaptosomes, they were fixed, and their membranes were permeabilised. First, they were incubated in a formaldehyde (Pierce™ 16% Formaldehyde (w/v), Methanol-free, Thermo Fischer Scientific, Cat. 28906) solution (4:100 by volume in PBS) for 10-minutes, followed by quenching with 20 mM glycine for another 10-minutes. Then the samples were washed twice with PBS and incubated in a permeabilising solution consisting of Triton-X (Sigma-Aldrich, Cat. X100-5ML) dissolved in PBS (1 in 100,000 by volume) for 5-minutes, followed by two washes with PBST. Then, the monoclonal anti-bassoon (abcam, Cat. ab82958) antibody was used to identify the pre-synaptic compartments, while the post-synapse was identified using anti-postsynaptic density (PSD)95 (abcam, Cat. ab18258). The antibodies were labelled with Alexa Fluor™ 488 and 647 NHS ester (Thermo Fischer Scientific, Cat. A20000 and A37573, respectively). The antibodies were incubated on the surface at 5 nM concentration for 20 minutes.

Bassoon was used in these experiments as a pre-synaptic marker due to its selective immunoreactivity in the pre-synaptic boutons throughout the brain.[66] PSD95 instead was used as a marker for the post-synapse, due to its specific immunoreactivity in the post synapse.

In order to image the αSyn, Aβ, and AT8-positive tau aggregates, monoclonal 4B12 (Thermo Fisher Scientific; Cat. MA1-90346), 6E10 (BioLegend; Cat. 9340-02), and AT8 (Invitrogen; Cat. MN1020B) antibodies labelled with Alexa Fluor™ 647 NHS ester were used at 5 nM, 1 nM, and 2 nM concentration and 30 minutes, 45 minutes, and 15 minutes incubation time, respectively.

*d*STORM imaging

*d*STORM images were acquired following a previously published protocol[41] on a custom-built single molecule localisation microscope (NanoPro) whose architecture and operation have been previously described in detail.[58] Briefly, a laser diode (PD-01229, LaserTack GmbH, Germany) emitting at 638 nm and operating at 420 mW was focused onto a 70 mm x 70 mm squared-core multimode fibre (05806-1 Rev. A, CeramOptec GmbH, Germany) agitated using a brushless DC motor (304-111, Precision Microdrives, UK) operated at <14,000 rpm. Light exiting the fibre was collimated and then focused at the back focal plane of an apochromatic, 100x, 1.49 numerical aperture objective (MRD01991, Nikon, UK). The excitation was translated to illuminate the sample under Total

Internal Reflection Fluorescence (TIRF). Emitted fluorescence was then collected onto a scientific Complementary Metal Oxide Semiconductor (sCMOS) camera (O1_PRIME_BSI_EXP, Teledyne Photometrics, UK). For each field of view, 2,000 frames were acquired at an exposure time of 50 ms.

Image processing and analysis

The acquired images were processed using the Aggregate Characterisation Tool (ACT).[54] Briefly, images were thresholded, dilated, and eroded to segment single molecules. The location of segmented molecules was calculated using ThunderSTORM,[55] and super-resolved images were calculated by super-imposing Gaussian-blurred localisation with localisation precisions of less than 20 nm.

The CellMask images were used to distinguish the synaptosomes using a custom segmentation protocol. Before imaging the synaptosomes, images of TetraSpeck fluorescent spheres (ThermoFisher, Cat. T7279, 1:1000 in PBS) in the same field-of-view (FoV) were obtained in both the CellMask (561 nm) and antibody (640 nm) channels. These images were used to generate an affine matrix, which was then applied to the CellMask images of the synaptosomes to correct the aberration-induced misalignment between the two channels. The corrected CellMask images were firstly thresholded, and the objects of interest were identified by selecting the regions where the intensity was higher than the average plus twice the standard deviation intensity within the FOV. Small objects induced by noise were removed by erosion and dilation operations. The remaining objects were size-filtered and circular spots with a diameter between 0.7 and 2.2 micrometres were identified as individual synaptosomes. A similar strategy was previously employed to segregate different synaptic compartments.[67–69]

Next, a density-based clustering algorithm (DSBCAN)[56] with two minimum points and 75 nm epsilon distance was performed on the super-resolution localisations in the 640 nm channel to cluster localisations into aggregates. Specifically, clusters with centroids within the identified synaptosomes were tagged as synaptic clusters, whereas those outside were labelled as extra-synaptic. Finally, the morphological features of these individual clusters were extracted and analysed.

QUANTIFICATION AND STATISTICAL ANALYSIS

The R Project Statistical Computing version 4.2.2 (2022-10-31)-" Innocent and Trusting" was used for all statistical analyses, the graphs were generated in GraphPad Prism 7.0a for Mac OS X, and the cartoon figures were created with BioRender.com. Representative aggregate images on Figure 3 were segmented using MetaMorph software v7.10.5.476 (Molecular Devices).[67,70] For the control experiments presented on Figure 2, three independent experiments using different brain samples and SiMPull coverslips were performed, and the data were collected for a total of 70 fields of views. For the human (Figure 4) and mouse (Figure 5) experiments, synaptosomes harvested from at least three independent brains on different days were tested on different coverslips. The number of synaptosomes studied in these experiments have been reported in the figure legends. Since the main goal of this study was to characterise the pathological aggregates inside the synaptosomes, the synaptosome itself has been treated as the experimental unit. The large number of synaptosomes used made it possible to use statistical tests with a requirement of normal distributions for sample sizes below 30, due to the law of large numbers.[71,72] Linear mixed effects models, ANOVA's with Type 2 sums of squares, and 95% confidence intervals (CI) were used to determine the differences between the groups (Tables S1 and S2). The datasets generated and analysed during the current study are available from the corresponding author on reasonable request. The code generated for the analysis of the super-resolved images can be accessed at https://github.com/jdanial/SynPull.

For data modelling and in order to produce the predictions in Figure 7, the Poisson distribution was used, given by the probability mass function

$$P(k) = \frac{\lambda^k e^{-\lambda}}{k!}$$

where k is the number of aggregates per synaptosome in question and λ is the average number of aggregates per synaptosome. This describes the distribution of independent events, given their average number, λ, and is expected to describe the number of aggregates per synaptosome if they appeared independently of each other, and with the same probability in each synaptosome. The solid grey line is produced by setting λ = -log(f0) where f0 is the experimentally measured fraction of synaptosomes with no aggregates. The dashed black line is produced by setting λ equal to the experimentally measured mean number of aggregates per synaptosome. The plots were produced in Python using the matplotlib and scipy packages.